24th IMEKO TC4 International Symposium
22nd International Workshop on ADC and DAC Modelling and Testing
IMEKO TC-4 2020
Palermo, Italy, September 14-16, 2020

DMPPT experimental demonstration unit based on Buck converter

Marco Balato, Annalisa Liccardo, Carlo Petrarca

Department of Electrical and Information Technologies, University of Naples Federico II Via Claudio 21, Napoli (NA), Italy
marco.balato@unina.it

***Abstract*— Distributed Maximum Power Point Tracking (DMPPT) technique represents the most promising solution to enhance the lackluster energetic performance of the mismatched PhotoVoltaic (PV) systems. Despite that, there are several factors which restrict its performance some of which are still to be explored. To fully understand the advantages offered by the DMPPT solution, the implementation of a DMPPT emulator is necessary. Based on the above needs, this paper describes the realization and use of a DMPPT experimental demonstration unit based on the Buck DC/DC converter. The above device is capable to emulate the output current vs. voltage (I-V) characteristics of many commercial PV modules with a dedicated Buck DC/DC converter not only in controlled atmospheric conditions but also with different currents rating of the switching devices. The system implementation is based on a commercial power supply controlled by a low-cost Arduino board. Data acquisition is performed through a low-cost current and voltage sensor by using a multichannel board by National Instruments. Experimental results confirm the validity and potential of the proposed DMPPT emulator.**

Keywords*— *Distributed maximum power point tracking; mismatching; PV emulator.

I. INTRODUCTION

The media battles of the Swedish teenager Greta Thunberg are awakening the consciences of millions of people on the global climate crisis; crisis that may be overcome through the achievement of the carbon neutrality. In this direction, the total production of electricity using renewable energy sources represents the main challenge. To increase the distributed green energy generation, PhotoVoltaic (PV) systems are among the most promising renewable sources. In the last 20 years, the main objective of the scientific community has been to fully explore the factors that limit the energetic performance of the mismatched PV systems [1–8] and propose possible solutions [9–41]. In particular, when mismatching conditions occur, due to clouds, shadows, dirtiness, different orientation of PV modules etc., the commonly used grid-connected PV systems, made of string of PV modules connected in parallel and feeding a central inverter, are ineffective. In order to face the above limitations, several solutions have been presented in the literature ranging from high-performance Maximum Power Point Tracking (MPPT) techniques [9–19] to reconfiguration architectures [20–29]. Among of all these techniques, the Distributed Maximum Power Point Tracking (DMPPT) approach is by far the most hopeful solution to improve the energetic performance of mismatched PV systems [30–41]. Despite that, there are still several factors which restrict its energetic performance, including the efficiency of the power stage, constraints imposed by the topology, the finite rating of silicon devices, atmospheric conditions, and the suboptimal value of string voltage [39–43]. The fact that many of these factors are not under our control represents a severe restriction in conducting experimental test activities when real DMPPT PV systems are considered. What emerges is the necessity of the implementation of DMPPT emulator. The present paper describes the realization and use of a DMPPT experimental demonstration unit based on the Buck DC/DC converter. The above device is capable to emulate the output I-V characteristics of many commercial PV modules with a dedicated Buck DC/DC converter not only in controlled environment conditions (as happens for common PV emulators [42–45]) but also with different currents rating of the switching devices. The high flexibility offered by the proposed device makes it suitable for testing traditional or innovative solutions such as the DMPPT and the reconfiguration approach, or a combination of both [41]. The system implementation consists of a commercial power supply controlled by a low-cost Arduino board. The control strategy is based on a set of equations defining the mathematical model of a DMPPT device. The paper is organized as follows: the mathematical model of a single Buck based DMPPT unit is described in detail in Section 2; section 4 is dedicated to the design and description of the proposed Buck based DMPPT emulator; experiments and tests are presented in Sections 4; and finally, Section 5 draws the conclusions.

II. MATHEMATICAL MODEL OF BUCK BASED DMPPT EMULATOR

The system shown in Fig. 1 will be considered and analyzed. The above system is composed by a PV module equipped with its own Buck DC/DC converter that realizing the DMPPT function. To simplify the readability of the following discussion, the considered system will be indicated with the acronym “B-PVU” that means Buck based

PhotoVoltaic Unit.

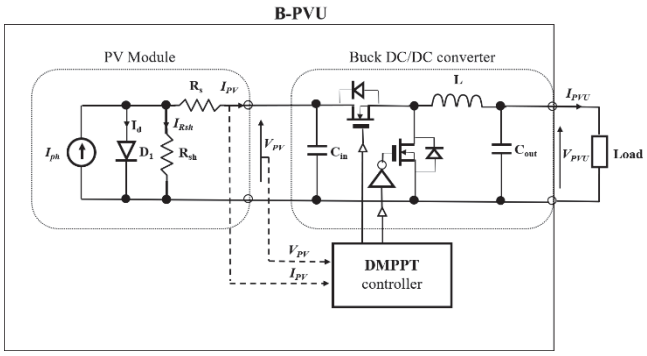

Figure 1: Circuit model of B-PVU.

In the above figure, $\boldsymbol{I_{PV}}$ ($\boldsymbol{V_{PV}}$) and $\boldsymbol{I_{B-PVU}}$ ($\boldsymbol{V_{B-PVU}}$) denote currents (voltages) at the input and output ports of the Buck DC/DC converter, respectively. Moreover, the symbol $\boldsymbol{P_{PV}}$ ($\boldsymbol{P_{B-PVU}}$) indicates the power extracted from PV module (B-PVU). Moreover, as shown in the Fig. 1, a single diode model of PV module will be considered in which the current generator represents the photo-induced current; diode D1 takes into account the effects at the silicon p–n junction of a PV cell; the series ($\boldsymbol{R_S}$) and parallel ($\boldsymbol{R_{sh}}$) resistances take in to account the loss mechanisms taking place in the PV module due to metallic ribbon. The typical output static Current vs. Voltage (I-V) characteristics of a PV module (dashed line) and of a B-PVU (bold line) are reported, at constant irradiance (S) and temperature (T) values, in Figure 2. Losses occurring in the power stage of the Buck converter (switching, conduction, and iron losses) and the settling time of the step response of a closed or open loop B-PVU are neglected. In addition, the MPPT efficiency of the DMPPT controllers is supposed to be equal to one ($\boldsymbol{\eta_{DMPPT} = 1}$). In these hypotheses, the output static I-V characteristic of a single B-PVU is marked by the presence of three different operating regions: Best Operating Region (BOR), and two Worst Operating Regions (WOR1 and WOR2). The adjectives best and worst are not used randomly insofar as they allow to discriminate operating points with high efficiency with respect to the other ones.

Worst Operating Region 1: In the WOR1, defined for $0 \leq V_{B-PVU} \leq V_1$, the output I-V characteristic of the B-PVU is flat and equal to:

$$I_{B-PVU} = I_{DSMAX} \tag{1}$$

where I_{DSMAX} indicates the maximum allowed current provides by the silicon devices. To explain the meaning of the voltage value V_1 some preliminary considerations are necessary. Since a Buck converter is able to lower its output voltage V_{B-PVU} with respect to the input voltage V_{PV}, and by considering that, when the PV module is working in its MPP, it must be:

$$V_{B-PVU} \cdot I_{B-PVU} = P_{MPP} \tag{2}$$

Where P_{MPP} is MPP power. It is evident that, as long as the PV module operating point matches the MPP, the lower the output voltage the higher the output current. By indicating with I_{DSMAX} the maximum allowed value of I_{B-PVU} without harming any silicon devices (power mosfets) we get:

$$V_1 = \frac{P_{MPP}}{I_{DSMAX}} \tag{3}$$

Therefore, V_1 is the lower limit of the output voltage V_{B-PVU} when the output power P_{B-PVU} assumes its maximum value and it can be calculated by using eq. (3) once I_{DSMAX} is known. In practice, the information regarding the value of I_{DSMAX} is included in the silicon devices 'datasheet.

Best Operating Region: BOR, defined for $V_1 \leq V_{B-PVU} \leq V_{MPP}$ is described by a hyperbole of Eq. (4), where $\mathbf{V_{MPP}}$ is the MPP voltage.

$$I_{B-PVU} = \frac{P_{MPP}}{V_{B-PVU}} \tag{4}$$

As shown in Figure 2, the current range (R_{BOR-I}) associated with BOR is defined as follows:

$$R_{BOR-I} = [I_{MPP}, I_{DSMAX}] \tag{5}$$

Worst Operating Region 2: WOR2 is defined for $V_{MPP} \leq V_{B-PVU} \leq V_{OC}$, where V_{OC} is the open circuit voltage that can be provided by the adopted PV module in the considered atmospheric conditions:

$$V_{OC} = V_{OC_{STC}}\left[1 + \frac{\alpha_V}{100}(T - T_{STC})\right] \tag{6}$$

Where the $V_{OC_{STC}}$ (T_{STC}) is the open circuit voltage (temperature) in the Standard Test conditions (S_{STC} =1000 W/m2, $T_{STC} = 25℃$) and α_V is the voltage temperature coefficient. In such a region, the characteristic of the controlled PV module coincides with the PV module one. In particular, for $V_{MPP} \leq V_{B-PVU} \leq V_{OC}$, the DMPPT controller forces the Buck DC/DC converter to work with a duty cycle equal to one. In this condition the current I_{B-PVU} is equal to:

$$I_{B-PVU} = I_{PV} = I_{ph} - I_d - I_{Rsh} \tag{7}$$

where I_{ph} is the photo-induced current, which, in accordance with Eq. (8), is linearly dependent on the irradiance level (S) and the PV module temperature (T), I_d is the current in diode D1 (Eq. (9)), and I_{Rsh} is the shunt-resistor current (Eq. (10)):

$$I_{ph} = I_{SC_{STC}}\frac{S}{S_{STC}}\left(1 + \frac{\alpha_I}{100}(T - T_{STC})\right) \tag{8}$$

$$I_d = I_{sat}\left(e^{\frac{V_{PV}+R_S I_{PV}}{V_T}} - 1\right) \tag{9}$$

$$I_{Rsh} = \frac{V_{PV}+R_S \cdot I_{PV}}{R_{sh}} \tag{10}$$

where V_T is the thermal voltage, α_I is the current temperature coefficient and I_{sat} is the diode reverse bias saturation current (Eq. (11)):

$$I_{sat} = CT^3 e^{\left(-\frac{E_{gap}}{kT}\right)} \quad (11)$$

where $k = 1.38$ J/K is the Boltzmann constant, E_{gap} is the band gap of the semiconductor material (in the following it is assumed $E_{gap} = 1.124$ eV), and C is the temperature coefficient [46]. The I-V output characteristics of a single B-PVU are strictly dependent on the irradiance and temperature levels (Eq. (12)). Typical curves are shown in Fig. 3.

$$T = T_{ambient} + \frac{NOCT-20}{800} S \quad (12)$$

Since in real environmental conditions the temperature usually changes quite slowly with respect to variation of the irradiance level occurring during the day, all subsequent results were obtained by considering a constant value of the PV module temperature equal to 57.5°C ($T = 57.5$ °C) which corresponds ($T_{ambient} = 25$ °C). In the following analysis a commercial PV module (Sunmodule SW225 [47]) will be considered, whose electrical characteristics in Standard Test conditions (STC) are reported in the Table 1.

Table 1. SolarWorld SW 225 PV module electrical characteristics in standard test conditions (STC).

($S_{STC} = 1000\ W/m^2, T_{STC} = 25\ °C$).

Description	Value
STC open circuit voltage	$V_{OC_{STC}} = 36.7\ V$
STC short circuit current	$I_{SC_{STC}} = 8.13\ A$
STC maximum power point voltage	$V_{MPP_{STC}} = 29.7\ V$
STC maximum power point current	$I_{MPP_{STC}} = 7.59\ A$
Voltage temperature coefficient	$\alpha_V = -0.34\%/K$
Current temperature coefficient	$\alpha_I = 0.034\%/K$
Nominal Operating Cell Temperature	$NOCT = 46\ °C$

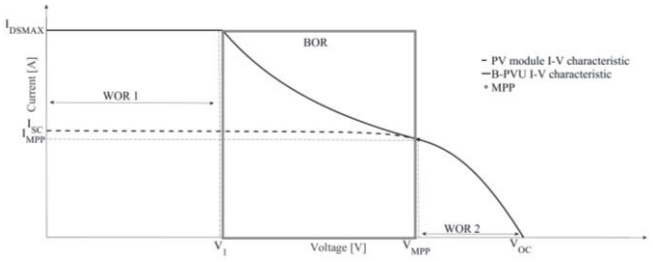

Figure 2. PV module I-V characteristic and B-PVU I-V characteristics.

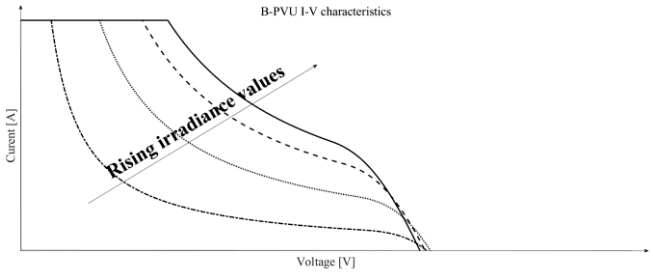

Figure 3. I-V characteristics of B-PVU.

III. IMPLEMENTATION OF B-PVU EMULATOR

A block diagram of the proposed B-PVU emulator is shown in Fig. 4.

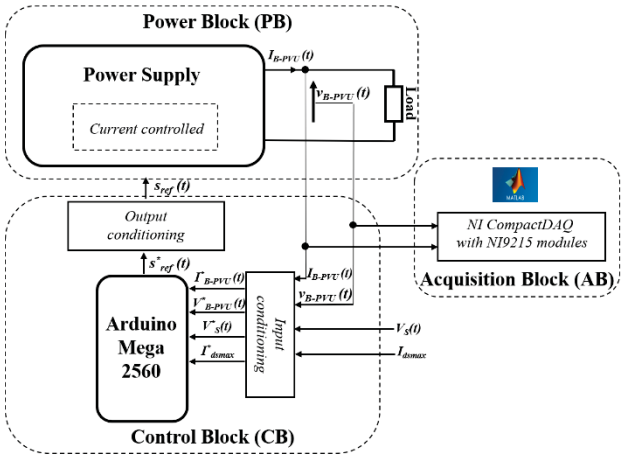

Figure 4: Block diagram of proposed B-PVU emulator.

It consists in three fundamental blocks: Power Block (PB), Control Block (CB) and Acquisition Block (AB).

Power Block (PB): PB consists of two commercial power supplies (Kepco BOP 100-4 [48]). One represents the power stage of the B-PVU emulator and is used as a current-controlled source whose output current $I_{PVU}(t)$ is regulated by means of a proper controller. The other one consists in a controlled electronic load able to proper scan the I-V characteristics of the B-PVU emulator. The two power supplies are suitable to work in all four quadrants of the current–voltage plane. They are linear power supplies with two bipolar control channels (voltage or current mode), selectable and individually controllable by either front panel controls or remote signals. The input signal of the PB (Sref (t)) is achieved based on the following equation:

$$S_{ref}(t) = S(t) \cdot I_{B-PVU} \quad (13)$$

Where $\boldsymbol{S(t)}$ represents the time varying irradiance value. Concerning the value of $\boldsymbol{I_{B-PVU}}$, it is obtained according to the eqs. (1), (4) and (7).

Control Block (CB): CB consists of controlling and conditioning units. The embedded board "Arduino Mega 2560" is used as controlling unit. The "Arduino Mega 2560" is powered via a USB connection and provides 54 digital input/output pins (15 of which can be used as PWM outputs) and 16 analog inputs, and it can be programmed through Arduino IDE software [49]. The analog input signals of the microcontroller, which are marked with an asterisk (Fig. 4), represent a scaled version of the corresponding signals $V_{PVU}(t)$, I_{PVU} (t), $V_S(t)$ and I_{DSMAX}. Such scaling is necessary to adapt the electrical characteristics of the above signals to the limited range [0,5] V of the microcontroller. Regarding the conditioning units, they are divided in: (a) the input conditioning unit and (b) the output conditioning unit. The input condition unit consists of a voltage (current) sensor for sensing and adapting the PVU output voltage (VPVU(t)) (current IPVU(t)) to the maximum allowed input voltage ($V^*_{PVU}(t)$ and $I^*_{PVU}(t)$) and a National Instruments generation

board (BNC-2100 series connector blocks), which is used to reproduce the input signals $V_S^*(t)$ and I_{DSMAX}^*. On the basis of the above discussion, the Arduino's input signals must fulfill the following equations:

$$V_{PVU}^*(t) = 5 \cdot \frac{V_{PVU}(t)}{V_{MAX}} \in [0,5]V \quad (14)$$

$$I_{PVU}^*(t) = 5 \cdot \frac{I_{PVU}(t)}{I_{MAX}} \in [0,5]V \quad (15)$$

$$V_S^*(t) = 5 \cdot \frac{\alpha_S \cdot S(t)}{S_{STC}} \in [0,5]\ V \quad (16)$$

$$I_{DSMAX}^* = 5 \cdot \frac{I_{dsmax}}{I_{MAX}} \in [0,5]V \quad (17)$$

where V_{MAX} = 50 V and I_{MAX} = 4 A are the maximum allowed values of the output voltage and current from the power unit; $\alpha_S = 1$ [V m^2/W]. The adopted current sensor is an "INA169 current sensor module", which allows measurement of continuous current up to 5 A. To reduce the PVU output voltage up to 10 times compared to the original, a voltage divider using resistance of 220 kΩ and 11.5 kΩ was adopted as a voltage sensor. At the end, the output conditioning unit consists in a Digital Analog Converter (DAC) "Adafruit MCP4725".

Acquisition Block (AB): AB consists in a commercial National Instruments multichannel USB data acquisition system (NI CompactDAQ with NI9215 modules characterized by 16-bit resolution and maximum sampling frequency of 100 kS/s) that allows to back up the experimental data in Matlab environment.

The experimental setup was designed and built in the Circuit Laboratory of the University of Naples Federico II and is shown in Fig. 5.

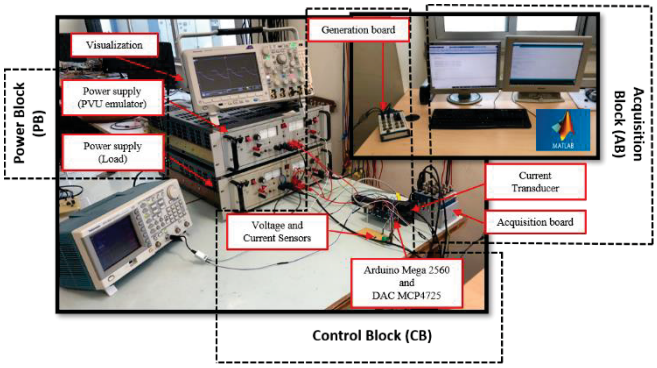

Figure 5. Experimental setup of proposed B-PVU emulator.

In the Table 2, the electrical characteristics of the proposed B-PVU emulator are reported.

Table 2. Electrical characteristics of the proposed B-PVU emulator.

Maximum output Current	$I_{B-PVUmax} = 5\ A$
Maximum output Power	$P_{B-PVUmax} = 150\ W$
Maximum output Voltage	$V_{B-PVUmax} = 36\ V$

In both figures, that represent a preliminary test results, a periodic (frequency 1 Hz) ramp signal has been applied at the microcontroller input $V_{PVU}^*(t)$ to scan the I-V characteristic of the proposed B-PVU emulator. The amplitude of the adopted ramp signal varies from 0 V to 3.3 V which corresponds to B-PVU ramp voltage $V_{B-PVU}(t)$ from 0 to V_{OC} ($V_{OC} = 33\ V$) that is the open circuit voltage at T = 57.5 °C (eq.(12)).

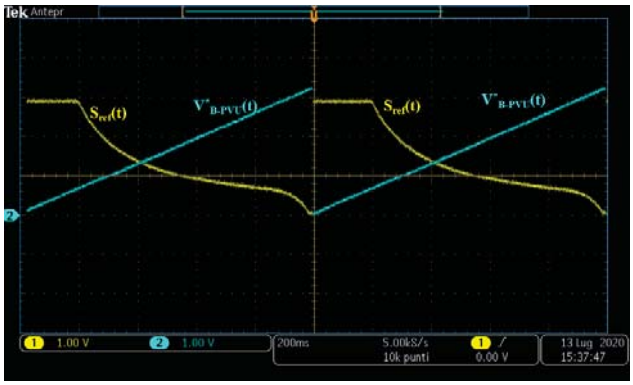

Figure 6. Oscilloscope screenshot (S=200 W/m^2, T=52.7°C, I_{DMAX}=3A).

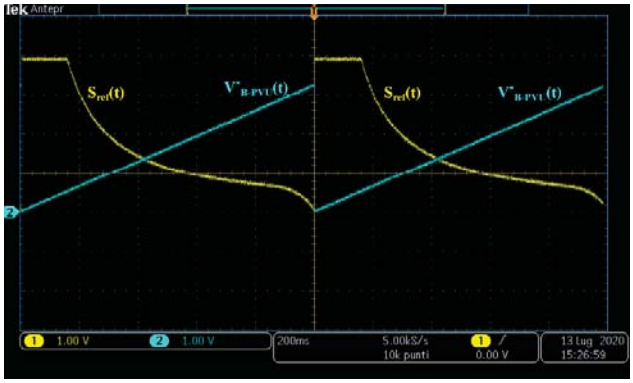

Figure 7. Oscilloscope screenshot (S=200 W/m^2, T=52.7 °C, I_{DMAX}=4A).

The different time domain behavior of $S_{ref}(t)$ (corresponding to the output signal of the DAC) reported in Figures 6 and 7 is linked to the adoption of two different values of I_{DSMAX}. In particular, in Figures 6 and 7 the value of I_{DSMAX} is equal to 3 A and 4 A. Further work is in progress in order to broaden the experimental analysis.

IV. CONCLUSIONS

In this paper, a DMPPT experimental demonstration unit based on the Buck converter has been presented and discussed. A detailed study was carried out in order to clearly understand the set of equations on which the mathematical model of the B-PVU is based on. The proposed emulator was designed to reproduce the I-V characteristics at different values not only of the irradiance levels but also of the value of I_{dsmax}. The high flexibility offered by the proposed solution allows to fully explore the performance of the DMPPT approach in the academic laboratories. Moreover, the possibility to swap the value of I_{dsmax} allows emulation of a large number of Buck converters, which results in a consistent reduction in time and cost. In particular, the proposed device represents a suitable compromise between

time and cost insofar as the inexpensive choice to adopt a commercial power supply is compensated by the possibility to emulate the behavior of many commercial devices. The proposed preliminary experimental results fully confirm the validity of the proposed emulator.

References

[1] Kaushika, N. D., and Rai, A. K., 2007, "An Investigation of Mismatch Losses in Solar Photovoltaic Cell Networks," Energy, 325, pp. 755–759.

[2] Baltus, C. W. A., Eikelboom, J. A., and Van Zolingen, R. J. C., 1997, "Analytical Monitoring of Losses in PV Systems," Proceedings of the 14th European Photovoltaic Solar Energy Conference, Barcelona, Spain, pp. 1547–1550.

[3] Bucciarelli, L. L., Jr., 1979, "Power Loss in Photovoltaic Arrays Due to Mismatch in Photovoltaic Cell Interconnection Circuits," Sol. Cells, 25, pp. 73–89.

[4] Bernieri, A., Betta, G., Ferrigno, L., Laracca, M., Schiano Lo Moriello, R., 2013, "Electrical energy metering: Some challenges of the European Directive on Measuring Instruments (MID)", Measurement: Journal of the International Measurement Confederation, vol. 46, n. 10, p. 3347-3354.

[5] King, D. L., Boyson, W. E., and Kratochvil, J. A., 2002, "Analysis of Factors Influencing the Annual Energy Production of Photovoltaic Systems," Proceedings of the 29th IEEE Photovoltaic Specialists Conference, New Orleans, LA, pp.1356–1361.

[6] Zilles, R., and Lorenzo, E., 1992, "An Analytical Model for Mismatch Losses in PV Arrays," Int. J. Sustainable Energy, 13, pp. 121–133.

[7] Chamberlin, C. E., Lehman, P., Zoellick, J., and Pauletto, G., 1995, "Effects of Mismatch Losses in Photovoltaic Arrays," Sol. Energy, 543, pp. 165–171.

[8] P. Manganiello, M. Balato, and M. Vitelli, "A survey on mismatching and aging of PV modules: The closed loop," IEEE T. Ind. Electron., vol. 62, no. 11, pp. 7276–7286, Nov. 2015.doi: 10.1109/TIE.2015.2418731

[9] D. Sera, L. Mathe, T. Kerekes, S. V. Spataru, and R. Teodorescu, "On the perturb-and-observe and incremental conductance MPPT methods for PV systems," IEEE J. Photovolt., vol. 3, no. 3, pp. 1070–1078, Jul. 2013.

[10] C.-S. Chiu, "T-S fuzzy maximum power point tracking control of solar power generation systems," IEEE T. Energy Conver., vol. 25, no. 4, pp. 1123–1132, Dec. 2010.

[11] Fontanella, R., Accardo, D., Schiano Lo Moriello, R., Angrisani, L., De Simone, D., 2018 , "An innovative strategy for accurate thermal compensation of Gyro Bias in inertial units by exploiting a novel Augmented Kalman Filter", Sensors (Switzerland), Vol.18, n.5.

[12] Buonanno, A., D'Urso, M., Prisco, G., Felaco, M., Angrisani, L., Ascione, M., Schiano Lo Moriello, R., Pasquino, N., 2013, "A new measurement method for through-the-wall detection and tracking of moving targets" Measurement: Journal of the International Measurement Confederation, vol. 46, n. 6, p. 1834-1848.

[13] Macaulay, J.; Zhou, Z. A Fuzzy Logical-Based Variable Step Size P&O MPPT Algorithm for Photovoltaic System. Energies 2018, 11, 1340.

[14] S. Kolesnik and A. Kuperman, "On the equivalence of major variable-step-size MPPT algorithms," in IEEE J. Photovolt., vol. 6, no. 2, pp. 590–594, March 2016. doi: 10.1109/JPHOTOV.2016.2520212.

[15] M. Sokolov and D. Shmilovitz, "A modified MPPT scheme for accelerated convergence," IEEE T. Energy Conver., vol. 23, no. 4, pp. 1105–1107, Dec. 2008. doi: 10.1109/TEC.2008.2001464.

[16] M. Balato, L. Costanzo, and M. Vitelli, "Maximum power point tracking techniques," in: Wiley Online Encyclopedia of Electrical and Electronics Engineering, John Wiley & Sons, New Jersey, February 15, 2016, pp. 1–26, https://doi.org/10.1002/0477134608X.W8299.

[17] G. Kumar, M. B. Trivedi, and A. K. Panchal, "Innovative and precise MPP estimation using P–V curve geometry for photovoltaics," Appl. Energ., vol. 138, no. 15, pp. 640–647, 2015.

[18] G. Kumar and A. K. Panchal, "Geometrical prediction of maximum power point for photovoltaics," Appl. Energ., vol. 119, no. 15, pp. 237–245, 2014.

[19] N. Femia, G. Petrone, G. Spagnuolo, and M. Vitelli, "Optimization of perturb and observe maximum power point tracking method," IEEE T. Power Electr., vol. 20, no. 4, pp. 963–973, 2005.

[20] D. Nguyen and B. Lehman, "An adaptive solar photovoltaic array using model-based reconfiguration algorithm," IEEE T. Ind. Electron., vol. 55, no. 7, pp. 2644–2654, 2008.

[21] L. F. L. Villa, D. Picault, B. Raison, S. Bacha, and A. Labonne, "Maximizing the power output of partially shaded photovoltaic plants through optimization of the interconnections among its modules," IEEE J. Photovolt., vol. 2, no. 2, pp. 154–163, Apr. 2012.

[22] H. Obane, K. Okajima, T. Oozeki, and T. Ishii, "PV system with reconnection to improve output under nonuniform illumination," IEEE J. Photovolt., vol. 2, no. 3, pp. 341–347, July 2012.

[23] Hideaki Obane, Keiichi Okajima, Takashi Oozeki, Takafumi Ishii: "PV System With Reconnection to Improve Output Under Nonuniform Illumination", IEEE Journal of Photovoltaics, vol. 2, no. 3, pp. 341-347, July 2012.

[24] J. Storey, P. Wilson, and D. Bagnall, "Improved optimization strategy for irradiance equalization in dynamic photovoltaic arrays," IEEE T. Power Electr., vol. 28, no. 6, pp. 2946–2956, June 2013.

[25] E. R. Sanseverino, T. N. Ngoc, M. Cardinale, V. Li Vigni, D. Musso, P. Romano, and F. Viola, "Dynamic programming and Munkres algorithm for optimal photovoltaic arrays reconfiguration," Sol. Energy, vol. 122, pp. 347–358, December 2015.

[26] D. La Manna, V. Li Vigni, E. R. Sanseverino, V. Di Dio, and P. Romano, "Reconfigurable electrical interconnection strategies for photovoltaic arrays: A review," Renewable and Sustainable Energ. Rev., vol. 33, pp. 412–426, 2014.

[27] M. Balato, L. Costanzo, and M. Vitelli, "Reconfiguration of PV modules: a tool to get the best compromise between maximization of the extracted power and minimization of localized heating phenomena," Sol. Energy, vol. 138, pp. 105–118, 2016.

[28] M. Balato, L. Costanzo, and M. Vitelli, "Series–

Parallel PV array re-configuration: Maximization of the extraction of energy and much more," Appl. Energ., vol. 159, no. 1, pp. 145–160, Dec. 2015.
[29] M. Balato, L. Costanzo, M. Vitelli, "Multi-objective optimization of PV arrays performances by means of the dynamical reconfiguration of PV modules connections (2015) 2015 International Conference on Renewable Energy Research and Applications, ICRERA 2015, art. no. 7418685, pp. 1646-1650.
[30] B. Burger, B. Goeldi, S. Rogalla, H. Schmidt: "Module integrated electronics e an overview", 25th European Photovoltaic Solar Energy Conference and Exhibition, September 2010, Valencia (Spain), pp. 3700-3707.
[31] Q. Li, P. Wolfs, A review of the single-phase photovoltaic module integrated converter topologies with three different DC link configurations, IEEE Trans. Power Electron. 23 (May 2008) 1320-1333.
[32] S.B. Kjaer, J.K. Pedersen, F. Blaabjerg, A review of single-phase grid-connected inverters for photovoltaic modules, IEEE Trans. Ind. Appl. 41 (5) (September-October 2005) 1292-1306.
[33] N. Femia, G. Lisi, G. Petrone, G. Spagnuolo, M. Vitelli, Distributed maximum power point tracking of photovoltaic arrays: novel approach and system analysis, IEEE Trans. Ind. Electron. 55 (7) (July 2008) 2610-2621.
[34] G.R. Walker, P.C. Sernia, Cascaded DC-DC converter connection of photovoltaic modules, IEEE Trans. Power Electron. 19 (4) (July 2004) 1130e1139.
[35] E. Roman, R. Alonso, P. Ibanez, S. Elorduizapatarietxe, D. Goitia, Intelligent PV module for grid-connected PV systems, IEEE Trans. Ind. Electron. 53 (4) (June 2006) 1066-1073.
[36] M. Balato, L. Costanzo, P. Marino, G. Rubino, L. Rubino, and M. Vitelli, "Modified TEODI MPPT technique: theoretical analysis and experimental validation in uniform and mismatching conditions," IEEE J. Photovolt., vol. 7, no. 2, pp. 604–613, 2017.
[37] C. A. Ramos-Paja, R. Gira, and E. I. Arango-Zuluaga "Distributed maximum power point tracking in photovoltaic applications: active bypass DC/DC converter," Rev. Fac. Ing. Univ. Antioquia., no. 64, pp. 32–44, 2012.
[38] M. Balato, M. Vitelli, "A new control strategy for the optimization of Distributed MPPT in PV applications", International Journal of Electrical Power & Energy Systems, Volume 62, 2014, Pages 763-773, ISSN 0142-0615.
[39] M. Balato, M. Vitelli, N. Femia, G. Petrone, and G. Spagnuolo, "Factors limiting the efficiency of DMPPT in PV applications," 2011 Int. Conf. Clean Electr. Power (ICCEP), Ischia, 2011, pp. 604–608.doi: 10.1109/ICCEP.2011.6036319.
[40] M. Balato, L. Costanzo, and M. Vitelli, "DMPPT PV system: modeling and control techniques," Adv. Renew. Energ. Pow. Technol., vol. 1, pp. 163–205, 2018.
[41] M. Balato, C. Petrarca, "The Impact of Reconfiguration on the Energy Performance of the Distributed Maximum Power Point Tracking Approach in PV Plants" Energies 2020, 13, 1511.
[42] M. Balato, L. Costanzo, D. Gallo, C. Landi, M. Luiso, M. Vitelli, "Design and implementation of a dynamic FPAA based photovoltaic emulator", Solar Energy, Volume 123, 2016, Pages 102-115, ISSN 0038-092X, https://doi.org/10.1016/j.solener.2015.11.006.
[43] Balato, M.; Liccardo, A.; Petrarca, C. Dynamic Boost Based DMPPT Emulator. Energies 2020, 13, 2921.
[44] Moussa, I.; Khedher, A.; Bouallegue, A. Design of a Low-Cost PV Emulator Applied for PVECS. Electronics 2019, 8, 232.
[45] N. Ullah, F. Nisar and A. A. Alahmadi, "Closed Loop Control of Photo Voltaic Emulator Using Fractional Calculus," in IEEE Access, vol. 8, pp. 28880-28887, 2020.
[46] N. Femia, G. Petrone, G. Spagnuolo, M. Vitelli, "Power Electronics and Control Techniques for Maximum Energy Harvesting in Photovoltaic Systems", 2012, CRC Press, Taylor & Francis group, ISBN: 978-1-4665-0690-9.
[47] Website: www.solarworld-usa.com/~/media/www/files/datasheets/sunmodule-plus/sunmodule-solar-panel-225-mono-ds.pdf.
[48] https://www.kepcopower.com/bop.htm.
[49] https://www.arduino.cc/en/main/software.